Single Objective Light Sheet Microscopy allows high resolution *in vivo* brain imaging of *Drosophila*

Authors

Francisco J. Tassara[1], Mariano Barella,[2] Lourdes Simó,[1] M. Mailén Folgueira Serrao,[1] Micaela Rodríguez-Caron,[1] Juan Ignacio Ispizua,[1] Mark H. Ellisman,[3] Horacio O. de la Iglesia,[4] M. Fernanda Ceriani[1*] and Julián Gargiulo.[1,5]*

Affiliations

1. Fundación Instituto Leloir, Buenos Aires C1405, Argentina
2. Adolphe Merkle Institute, University of Fribourg, Chemin des Verdiers 4, CH-1700 Fribourg, Switzerland
3. National Center for Molecular Imaging Research, Department of Neurosciences, School of Medicine, University of California, San Diego, La Jolla, CA 92093-0608, USA
4. Department of Biology, University of Washington, Seattle, WA 98195-1800, USA
5. Instituto de Nanosistemas, Universidad Nacional de San Martín, B1650 Buenos Aires, Argentina

*** jgargiulo@unsam.edu.ar**
*** fceriani@leloir.org.ar**

Abstract |

In vivo imaging of dynamic sub-cellular brain structures in *Drosophila melanogaster* is key to understanding several phenomena in neuroscience. However, a trade-off between spatial resolution, speed, photodamage, and setup complexity limits its implementation. Here, we designed and built a single objective light sheet microscope, customized for *in vivo* imaging of adult flies and optimized for maximum resolution. Unlike multi-objective light sheet setups, the microscope uses a single objective at the fly head interface, facilitating sample mounting and inspection, and reducing invasiveness. In contrast to two-photon microscopies, the light-sheet configuration with visible excitation offers reduced phototoxicity. We demonstrate *in vivo* imaging of the membrane, mitochondria, and dense-core vesicles in the axonal projections of

small lateral ventral neurons. The achieved resolution was between 380 to 500 nm within a field of view of 70×50×12 μm³. This unique combination of easy sample mounting, high resolution, and the low-phototoxicity of light sheet illumination paves the way for new dynamic studies in the brain of living flies.

MAIN TEXT

Introduction

Drosophila melanogaster is an ideal model to address key questions in neuroscience, given its relatively simple and genetically tractable nervous system. The recent availability of the fly brain connectome predicts new lines of research requiring live brain imaging of intact individuals.[1] The recent years have seen impressive advances in optical microscopy techniques, and the community has built expertise on how to create fly preparations for long-term optical brain imaging.[2–5] Using protein-based probes such as the GCaMP family,[6] it is possible to translate activity-dependant intracellular ion concentrations into fluorescent signals. With these tools, it has been possible to obtain *in vivo* neuronal activity maps in adult flies and to correlate them with sensorial stimuli, behavior and metabolism.[7] Neuronal activity mapping demands rapid (sub-second) whole-brain or large-volume imaging, targeting clusters of neurons—ranging from a few to tens of microns in size—that exhibit correlated activity. This approach aims to uncover large-scale communication networks within the brain.[8,9]

On the other hand, *in-vivo* imaging of dynamic sub-cellular anatomical structures such as individual neurites, cytoskeleton or organelles has been less explored but is the key to understand phenomena such as circadian structural plasticity,[10,11] time of day- dependent connectivity,[12,13] axonal regeneration and lesion recovery,[14] or the structural correlates that result from forced

depolarization/hyperpolarization.[15,16] This approach requires a different spatiotemporal scale. It aims to describe structures ranging from a few cents of nanometres to a few microns, and the demand for speed can be relaxed. Until now, this type of *in vivo* studies has been limited, and they typically use a different individual for each time point.[3] Here, we aim to bridge this technology gap using light sheet (LS) microscopy.

Until now, the most popular approach to *in vivo* brain imaging in *Drosophila* has been two-photon microscopy (2pM), where a highly focused pulsed laser is scanned through the sample.[17–19] The technique achieves high resolution and sectioning, and the use of infrared excitation wavelengths allows a deep penetration in the tissue. With 2pM, it was possible to acquire brain activity maps that are odor[2,4,20] auditory,[21] or visually-evoked,[22,23] during walking,[24,25] sleeping,[26] or eating.[27] In addition, it allowed the study of functional correlations between brain regions,[9] and its correspondences with metabolism.[28] However, 2pM has significant limitations for imaging living animals. Firstly, the use of high peak pulse powers can induce photodamage or brain heating,[29] or even behavioral responses.[24] Secondly, it is affected by substantial photobleaching that limits the number of volumes that can be acquired. Pulsed lasers can be avoided using one-photon microscopies such as confocal,[30] spinning disk[31,32] or epifluorescence with light-field[33,34]. However, these techniques can suffer from similar or even higher photobleaching. This can be mitigated by employing confocal scanning light-field microscopy, at the expense of optical and computational complexity.[35]

Most of the aforementioned drawbacks could be alleviated through the utilization of LS microscopy.[36,37] This technique enables the selective illumination of a specific imaging plane being imaged, thereby significantly reducing photobleaching and phototoxicity compared to

scanning methods. Furthermore, it does not require pulse lasers and is inherently faster than scanning methods because an entire plane is acquired in a single acquisition. LS microscopy has been successfully used in developing embryos[8] or other model organisms[38]. However, there are several challenges to implementing this technique for *in vivo* high resolution brain imaging in adult *Drosophila*. Firstly, it typically requires two or more objectives, which makes the interface with the fly's head more cumbersome. Secondly, placing two lenses at a given angle requires objectives with long working distances that are associated with low numerical apertures (NA), which reduces the spatial resolution. In addition, the necessity to rigidly maintain the alignment between illumination and detection optics usually requires the sample to be physically scanned through the sheet of light, limiting the speed of these techniques. For these reasons, the implementation of LSM to adult *Drosophila* has been limited to very low spatial resolution[39] or *ex vivo* preparations.[40]

Recently, Swept Confocally-Aligned Planar Excitation (SCAPE) microscopy leveraged the implementation of LSM to living adult animals such as mice,[41] *C. elegans*,[42] and zebrafish.[42] SCAPE belongs to a family of techniques called oblique plane microscopy (OPM) or Single Objective LS Microscopy (SOLS). These techniques use a single objective for both oblique LS illumination and imaging.[43–46] This feature greatly simplifies sample mounting and allows the use of a high NA objective. In addition, the sheet of light is rapidly scanned through the sample using galvanometric mirrors, eliminating the need to move the specimen. The SOLS system employs remote focusing to create a three-dimensional virtual image of the sample, which is then imaged with a tertiary microscope, tilted to match the angle of the oblique light sheet. Very recently, SCAPE demonstrated brain-wide calcium imaging of living *Drosophila* adults at 10

Hz.[47] However, their research focus was limited to clusters of neurons, with suboptimal spatial resolution and an imaging voxel size of (1×1.4×2.4) μm^3.

Here, we designed and built a SOLS microscope tailored for *in vivo* imaging of adult *Drosophila* and optimized for maximum resolution. Our design utilizes a bespoke glass-tipped objective for the tertiary microscope,[45] with almost no loss of spatial resolution at the remote imaging.[45,46] With it, we demonstrated *in vivo* imaging of the axonal projections of small lateral ventral neurons (s-LNvs), with a high spatial resolution of 500 nm. We imaged the plasma membrane, mitochondria and dense-core vesicles. The built microscope possesses the convenient sample mounting of confocal or 2p microscopy, as well as the typically gentle photobleaching of LS illumination.

Results

Experimental setup

Figure 1a shows the schematics of the SOLS microscope with oblique illumination. It is based on previous designs,[42,44,45,48] but optimized to facilitate the interface with the living fly, and to maximize spatial resolution. In short, it consists of an upright primary microscope with a water immersion objective O1 (60×, 1.1 NA) that excites the sample with oblique light-sheet illumination and collects the fluorescence emission, which is relayed by a remote focusing system that creates a virtual replica of the sample using secondary objective O2 (60×, 0.9 NA, air). A remote microscope equipped with a bespoke glass-tipped objective O3 (1.0 NA) is oriented at an angle and images the virtual replica. All microscope modules are configured as 4f optical systems. The experimental setup also features an epifluorescence wide field microscopy

module, useful for coarse sample positioning. A flip mirror (M') and a beam splitter (BS) can be placed on the excitation and detection paths to switch between the LS and wide field configurations.

To create the LS, the beam is shaped by the LS excitation module. To facilitate the description of the beam shaping and routing, Figure 1b shows the cross-section of the beam at selected planes, marked with dashed blue lines in Figure 1a. The excitation uses a fiber-launch system that combines two continuous-wave, linearly polarized, 488 nm and 561 nm lasers. An achromatic lens L1 (f=30 mm) collimates the beam to a circular Gaussian profile (Figure 1b, panel i). Then, the beam is reduced 5× in the *x*-axis by two cylindrical lenses, CL1 (f=250 mm) and CL2 (f=50 mm), as shown in Figure 1b, panel ii. A third cylindrical lens CL3 (f=100 mm) focuses the beam on the *y*-axis onto an adjustable mechanical slit, as shown in Figure 1b, panel iii. The slit is placed in a plane that is conjugated to the back focal plane of the objective O1 (Figure 1b, panel iv). In this way, the slit truncates the Gaussian beam in the *x*-axis, and the width of the slit controls the excitation NA of the LS. The entire LS excitation module is mounted on a translation stage that shifts off-axis the beam along the *x*-axis at the back focal plane of O1 by a magnitude Δx. This offset controls the LS angle θ. Figure 1b, panel v shows the focused beam at the back focal plan of O1 corresponding to the wide field module.

To achieve non-distorted remote focusing, the composed magnification M between the sample and its virtual replica must satisfy M=n_2/n_1, where n_1 and n_2 are the refractive index at the sample and image planes, respectively.[49,50] This is achieved by using a Tube Lens (TL2=135 mm) that is the assembly of three optical components (for details, see Methods and Millett-Sikking *et al.* [51]). Finally, the remote microscope is oriented so that its axis forms an angle θ

with respect to the O2 axis. In this way, the imaging plane is orthogonal to the excitation, which is the standard requirement in LS microscopy.

The scanning module uses a single axis-galvanometric mirror (GM) to perform lateral scanning of the LS through the sample in an angle-invariant way, as schematized in Figure 1c and explained in detail by Kumar *et al*.[52] The GM plane is conjugated to the back focal plane of both objectives O1 and O2. This configuration enables the GM to de-scan the fluorescence emission, keeping the virtual image generated by the remote focusing module stationary. During the scanning of the LS in the *x* direction, an image is acquired with the LS camera (CLS) for each LS position. This creates a 3D parallelepiped-shaped volume (Figure 1c, light green box) that is later computationally deskewed into the traditional cartesian coordinates system.

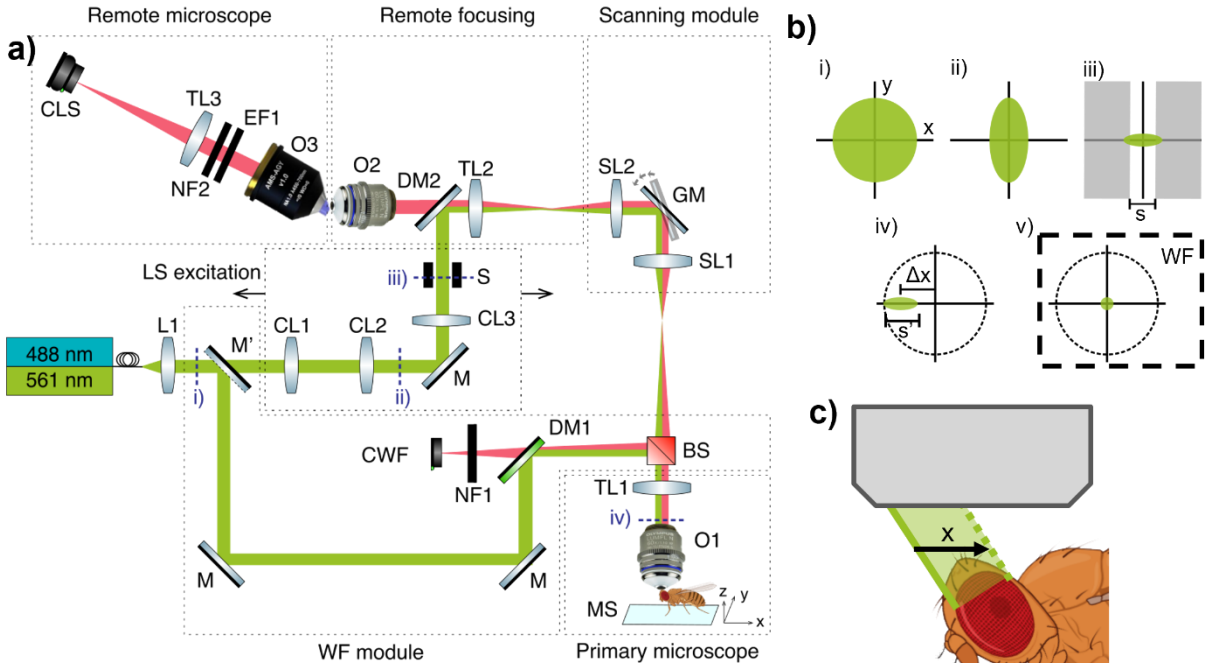

Figure 1: a) *Schematic of SOLS. The experimental setup is divided into main key modules: The LS excitation module shapes the laser beam for oblique plane illumination; the scanning module is responsible for sweeping the sheet of light across the sample; the primary microscope*

illuminates the sample and detects the fluorescence signal; the remote focusing system creates a virtual replica of the sample; the remote microscope images the replica. The microscope can be set in an epifluorescence wide field configuration (WF module) for coarse sample positioning. O1, O2 and O3: primary, secondary and tertiary objectives, respectively. TL1, TL2, TL3: Tube lenses. DM, DM2: Dichroic mirrors. CL1, CL2, CL3: Cylindrical lenses. M: mirror. M': Flip mirror. GM: Galvanometric mirror. BS: Beam splitter. SL1, SL2: Scanning lenses. CWF: Camera used in Epifluorescence mode. CLS: Camera used in Light Sheet mode. EF1, EF2: Emission filters. NF: Notch filter. MS: Motorized stage. Arrows in the LS excitation module depict that the module is built on top of a translation stage. ***b)*** *Sketch of the beam shape at different positions along the optical path. Panels i to v are not to scale and correspond to the planes indicated with blue dashed lines in (a). Panel v corresponds to the same plane as iv but for the Wide Field illumination. The real sizes of the beam at each panel, calculated as the Full Width Half Maximum in (x, y) are: i) (2.35, 2.35) mm, ii) (0.47, 2.35) mm, iii) (0.47 mm, focused). Slit width s=0.8 mm. iv) (s'=1.06 mm, focused), v) (focused, focused).* ***c)*** *Sketch representing the light sheet scan over the sample space.*

Instrument characterization

Figures 2a and 2b show the schematics of the illumination light sheet and its relevant dimensions. It is a truncated Gaussian beam with an incident angle θ with respect to the x-axis. The beam propagates parallel to the z' axis, is collimated in the yz' plane and is focused on the $x'z'$ plane. It is defined by a beam waist w_0, a width w_y and a length $L_{z'}$ in the x', y and z' axis, respectively. In SOLS microscopy - and LS microscopy in general - there is a trade-off between resolution, sectioning, axial field of view (FOV), and collection efficiency, which depends on the LS incident angle and NA. In this setup, we have optimized the design to maximize resolution

and sectioning, at the expense of axial FOV. The angle was set to θ=41°, following the criteria of matching the LS thickness to the axial point spread function (PSF) of the emission, as described by Millett-Sikking *et al.*[51]

The beam profile was characterized by scanning a single 100 nm fluorescent bead through the LS. For each position of the bead, the total detected fluorescence emission at the LS camera was calculated. Figure 2c illustrates the resulting normalized intensity map, acquired at an excitation wavelength of 561 nm. The measured angle is θ= (41 ± 1)°. Figure 2d shows an intensity map of the region closer to the beam waist. Figures 2e, 2f, and 2g show intensity linear profiles along the *y*, *z'* and *x*' axis, respectively. Measured values are w_0=(2.2 ± 0.1) µm and L_y=(53 ± 1) µm, calculated as the full widths at half-maximum (FWHM). In the propagation direction *z'*, L_z= (39 ± 1) µm is computed as twice the distance over which the intensity drops by a factor of $\sqrt{2}$.

The axial and lateral resolution were studied for both excitation lasers. For that, a 2D calibration sample consisting of individual beads drop-casted on a glass substrate was used (see Methods for details). The sample was placed in a series of *z* positions relative to the focal plane of the objective. For each *z* position, a 3D volume was imaged, and the PSF of each bead was analyzed. Representative PSFs are shown in Figure 2h for both excitation lasers at *z*=0. The full width at half maximum FWHM was computed for each bead in the three axes. Figure 2i shows the lateral FWHM for both lasers as a function of the z position of the sample. The lateral resolution is relatively uniform in an axial range of approximately 30 µm. The resolution is slightly better for the *x*-axis (solid lines) than for the *y*-axis (dashed lines). This is a typical feature of SOLS microscopy and is explained by a loss of effective detection NA in the direction of the tilt of the remote microscope.[42,45] At the focal plane, the resolution was ($FWHM_x$, $FWHM_y$) = (365 ± 6,

437 ± 3) nm, and ($FWHM_x$, $FWHM_y$) = (429 ± 3, 488 ± 5) nm for the 488 nm and 561 nm excitation, respectively. Figure 3j shows the axial resolution as a function of the z position of the sample. At the focal plane, the $FWHM_z$ are (1150 ± 40) nm and (1460 ± 30) nm for 488 nm and 561 nm excitation wavelengths, respectively. Away from this plane, the LS increases its thickness, deteriorating the axial resolution. The obtained values are consistent with the Rayleigh length R_l of the LS,[53] $R_l = n\pi w_0^2/(8\,\lambda\, ln2) = (6.5 \pm 0.3)$ µm.

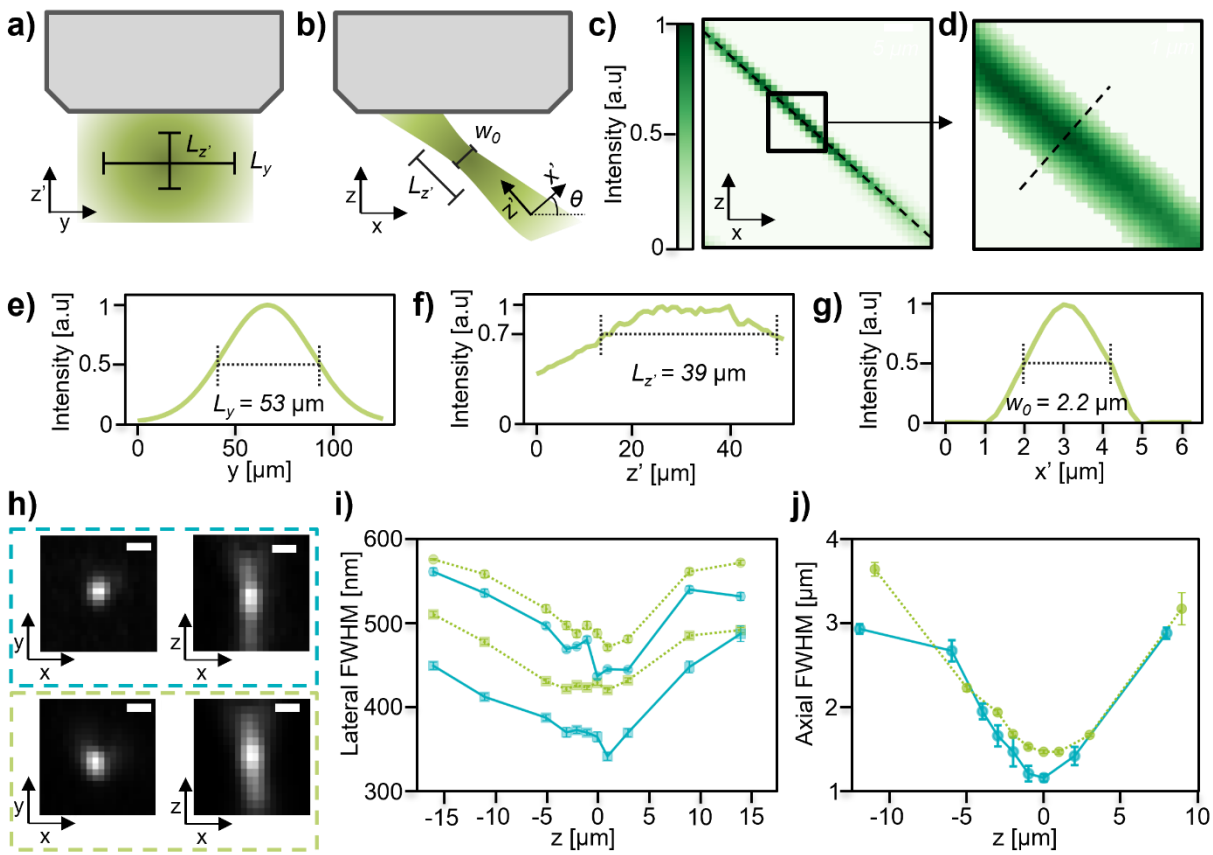

Figure 2: *Characterization of the excitation light sheet and the microscope resolution.* ***a)*** *and* ***b)*** *Sketch of relevant dimensions of the LS illumination.* ***c)*** *Normalized intensity of the measured light sheet beam in the xz plane.* ***d)*** *Detail of the light sheet beam waist shown in the black box of (c).* ***e-f)*** *Normalized intensity profiles of the LS in y, z' and x' axes, respectively.* ***h)*** *Top, blue dashed box: PSF cross-section in the xy and xz planes for a 488 nm excitation. Bottom, green*

dashed box: for a 561 nm excitation. Scale bar:1 µm. ***i)*** *Lateral PSF FWHM as a function of z for 488 nm (light blue solid line) and 561 nm (light green dashed line). Circular and square scatters represent the PSF width in the x and y directions, respectively.* ***j)*** *Axial PSF FWHM as a function of z for 488 nm in blue and 561 nm in green.*

High resolution imaging of sLNv neurons in living adult flies

To demonstrate the capabilities of the SOLS microscope in a living fly, the axonal projections of the small lateral ventral neurons (s-LNvs) were imaged. These neurons are a key component of the circadian clock in the *Drosophila* brain as they coordinate circadian activity in constant conditions.[54] They also release the PDF neuropeptide, which is necessary to maintain the internal coherence of the circadian network.[55] The somas of the s-LNvs are in the accessory medulla and project to the dorsal protocerebrum, where they contact other clusters of clock neurons.[56] These projections are very stereotyped and easy to observe as there are very clean drivers available which allow their manipulation and visualization. In addition, their projections are found approximately 25 µm below the brain surface, which makes them accessible during *in vivo* preparations.

For imaging, the fly is mounted on an aluminum foil with a hand-made triangular hole, as shown in Figure 3a. First, the fly is anesthetized on ice and gently manipulated to position the head and thorax into the hole using forceps under a dissection microscope. Then, the head of the fly is bent forward to give access to its posterior surface to later carefully immobilize by the eyes employing beeswax at 70 °C. Later, a small portion of the cuticle of the dorso-posterior region of the head is removed under saline solutions (mark with a dashed square in Figure 3a, see Methods for details). Finally, the air sacs and the fat tissue were also removed to obtain optical access to the s-LNv region. Importantly, the M16 muscle was cut to reduce brain motion.[57]

Transgenic flies expressing plasma membrane GFP in the s-LNv neurons were imaged (;UAS-mCD8::GFP;pdf-Gal4). 3D volumes were acquired at an excitation wavelength of 488 nm, with a field of view of 70×50×12 μm^3 and a voxel size of 0.12×0.12×0.16 μm^3. A representative top view (*xy*) of the right terminals of the s-LNv neurons is shown in Figure 3b, with the axial position color-coded. To show the resolving power of the microscope, Figure 3c shows some close-up of a few selected frames presenting small features. Figure 3d-i shows a line intensity profile of a selected thin process with a FWHM of 360 nm. Figure 3d-ii shows a line intensity profile across two resolved thin processes, separated by 640 nm. Furthermore, a parameter-free image resolution estimation based on decorrelation analysis was implemented, following the methods from Descloux *et al.*[47–49]. The estimated lateral resolution of the z-stack is (540 ± 10) nm (see further details in Methods). The algorithm does not distinguish between the *x* and *y* directions, and therefore the value corresponds to a lateral average resolution.

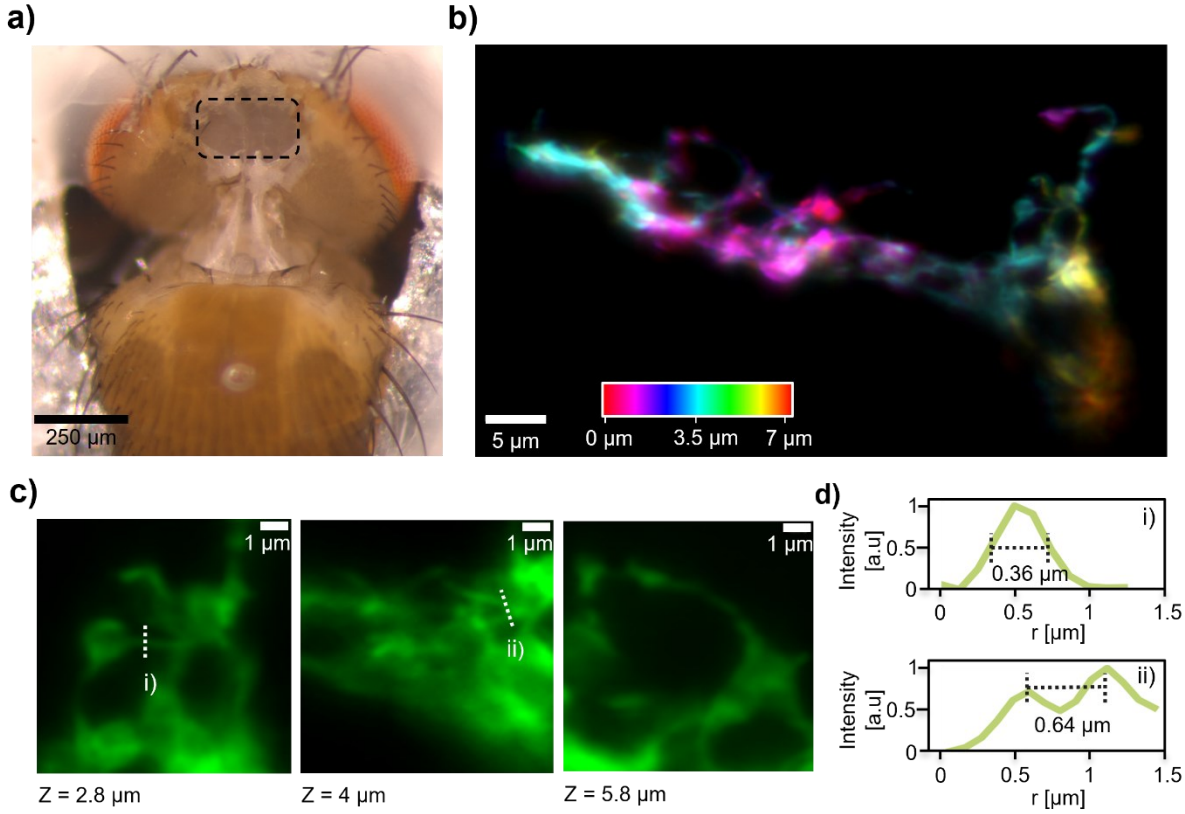

Figure 3: Imaging *fluorescent sLNv neurons in living adult flies.* ***a)*** *Image showing the mounted fly, highlighting the area where the cuticle dissection was performed with black dashed lines.* ***b)*** *Representative image of s-LNv terminals captured with the SOLS microscope, illustrating the structure of interest in flies expressing ;UAS-mCD8::GFP;pdf-Gal4.* ***c)*** *Magnified views of distinct regions within the terminals at selected axial frames, to reveal structural details.* ***d)*** *Intensity profiles across the white-dashed lines marked in (c)****.***

Then, two-color imaging of the s-LNv neurons was performed using the two available lasers. First, a fly expressing GFP in the plasma membrane and mKO fluorescent protein in the mitochondria was imaged. Figure 4a shows an example of a z-projection in an axial range of 7 μm. GFP is shown in green and mKO in red. Figure 4b shows a close-up of a single selected frame. Most of the red signal appears in small clusters with sizes ranging from 400 to 800 nm, which is consistent with the typical size of a mitochondrion. However, it is not possible to determine the number of mitochondria in one cluster. Then, a fly expressing GFP in the plasma membrane and mCherry in the dense core vesicles (DCVs) was studied. Figure 4c shows an example of a z-projection and Figure 4d shows a close-up of a single selected frame. Plasma membrane is shown in green and DCVs in magenta. In all images of Figure 4, a Richardson–

Lucy deconvolution algorithm was applied to increase the contrast and resolution.[58]

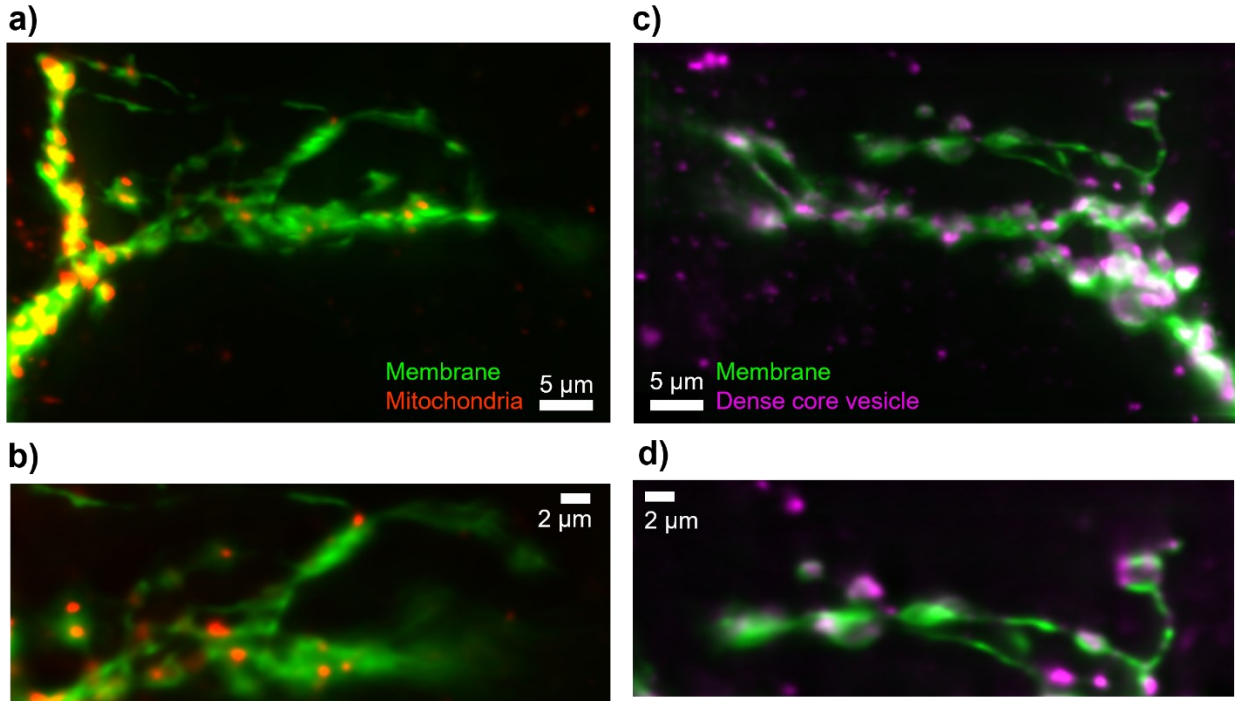

Figure 4: ***a)*** *Image of an sLNv terminal in a fly expressing ;UAS-mCD8::GFP;pdf-Gal4 > ;UAS-mito::mKO;. The membrane is labeled in green (GFP), while mitochondria are labeled in red (mKO).* ***b)*** *Magnified views of a single axial frame at a selected region from panel (a), showcasing finer structural details of the mitochondrial and membrane organization.* ***c)*** *Image of an sLNv terminal in a fly expressing ;UAS-mCD8::GFP;pdf-Gal4 > ;;UAS-sytα::mCherry. The membrane is labeled in green (GFP), and dense core vesicles are labeled in magenta (mCherry).* ***d)*** *Magnified views of a single axial frame at a selected region from panel (c), revealing the fine structural details of the vesicles and membrane organization. All images in this Figure went through a Richardson–Lucy deconvolution process with 10 iterations.*

Discussion

A 2-color upright single objective light sheet microscope was designed and built for imaging of living adult *Drosophila* flies. Because it utilizes a single objective at the interface with the flies' head, it offers a series of advantages with respect to other LS implementations that require several objectives such as lattice light sheet microscopy. First, it is compatible with an epifluorescence imaging module for simple sample finding and positioning. Secondly and more importantly, it is less invasive because it requires a smaller dissection area on the head´s cuticula, as it is only necessary to accommodate the light cone of a single objective. This can have a positive impact on the flies' health, which is crucial for long-term imaging experiments. Furthermore, this configuration also offers open space for other devices such as perfusion systems. These features were already available with the most standard technology for live imaging of *Drosophila* which is 2pM. However, LS microscopy is known for its characteristically lower photobleaching and avoids using high-power infrared pulses that are potentially phototoxic.

While it has been already demonstrated that SOLS microscopy is capable of achieving resolutions close to the diffraction limit on a series of biological systems such as zebrafish or *Drosophila* eggs,[46] here we have demonstrated it for brain imaging in a living adult fruit fly for the first time. A lateral resolution between 380 nm to 500 nm for 488 nm excitation was demonstrated in a field of view of 70×50×12 μm^3. Remarkably, this is comparable to the achievable resolutions of 2pM.[59,60] It must be noted that the lateral FOV can easily be extended to the entire FOV of the primary objective (200 μm for the 60× objective used in this work). Here we have used a smaller FOV to fit the size of the biological region of interest. The axial FOV can also be extended, but at the expense of axial resolution and sectioning.

Two-color imaging was demonstrated on the axonal terminals of sLNv neurons. We imaged flies expressing a fluorescent dye at the membrane in combination with either the mitochondria or the dense-core vesicles. This type of measurements could enable studies that correlate neuronal structure with the (dynamic) distribution of specific organelles of interest. This contrasts with most published research on live imaging of *Drosophila*, which typically studies calcium dynamics in response to external stimuli. In particular, long-term *in vivo* imaging of sLNv could provide insights into the circadian plasticity of these clock neurons.

Future improvements could include higher NA primary objectives for even higher resolution and optical throughput. In addition, this approach for live imaging is compatible with all the recent and expanding advancements of SOLS microscopy such as combination with optogenetic stimulation,[45] multi-view imaging,[46,61] live projection imaging,[62] Raman spectroscopy,[63] structured illumination,[64] or adaptive optics.[65]

Materials and Methods

Materials

Microscope components

O1: 60x, 1.1 NA, LUMFLN60XW, Olympus. **TL1:** SWTLU-C f =180 mm, Olympus. **O2:** 60x, 0.9 NA, air, MPLAPON60X, Olympus. **TL2:** Effective focal length 135 mm - TTL200MP + ACT508-750-A + ACT508-500-A, Thorlabs. **O3:** AMS-AGY-v1.0, Applied Scientific Instrumentation. **TL3:** TTL200-A - f = 200 mm, Thorlabs **SL1 and SL2:** f =70 mm CLS-SL, Thorlabs. **L1:** AC254-030-A-ML - f=30 mm, Thorlabs **CL1:** ACY254-250-A - f = 250.0 mm, Thorlabs **CL2:** ACY254-050-A - f = 50.0 mm, Thorlabs **CL3:** ACY254-100-A - f = 100.0 mm, Thorlabs. **GM:** Saturn 9B, ScannerMAX. **Lasers:** LBX-488 and LCX-561, Oxxius. **Cameras:** pco.edge 4.2 sCMOS, PCO and CS165MU/M - Zelux®, Thorlabs. **BS:** BSW26R 50:50,

Thorlabs. **DM1, DM2:** ZT405/488/561rpc-UF3, Chroma. **NF:** ZET488/561m, Chroma. **EF:** ET510/20m for 488 nm excitation and ET630/75m for 561 nm excitation, Chroma.

Subject details

All experiments were performed on adult flies, 2–5 days post-eclosion. Stocks ;*pdf*-Gal4;*pdf*-Gal4 (#80939), used as a driver for s-LNvs and ;UAS-mCD8::GFP; (#5137), used to label plasma membrane, were obtained from Bloomington Stock Center. ;;UAS-Sytα::mCherry, employed to label dense-core vesicles, was generously provided by Paul H. Taghert.[66] ;UAS-mito::mKO; was generated in our lab to label mitochondria.

Fly mounting and preparation

An aluminum foil with a hand-made hole was glued to the 3D-printed fly holder (Fig 3a), following published methods.[57] The fly was anesthetized on ice and under a dissection microscope, its head and thorax were positioned into the hole using forceps (Fine Science Tools). The head of the fly was bent forward to give access to its posterior surface and carefully immobilized by the eyes employing beeswax (70 °C, Sigma) and a thin-end wax carving pencil. Under saline solution (103 mM NaCl, 3 mM KCl, 5 mM TES, 8 mM trehalose, 10 mM glucose, 26 mM NaHCO3, 1 mM NaH2PO4, 4 mM MgCl2 and 1.5 mM CaCl2),[67] the cuticle in the dorso-posterior region of the head was removed employing sharpened #5 forceps and a tungsten needle (Fine Science Tools). The air sacs and the fat tissue were also removed to obtain optical access to the s-LNv region. The M16 muscle was cut to prevent brain motion.

Data acquisition

The microscope's components are controlled through a Python-based graphical user interface specifically programmed for image acquisition tasks. The acquisition sequence was adapted from the code available at the GitHub repository https://github.com/amsikking/SOLS_microscope. Image acquisition was synchronized via a National Instruments board, which managed the triggering between the camera and the galvo mirror driver. The exposure time for the volumes shown in Figures 3 and 4 was 100 ms per frame. This resulted in a total acquisition time of around 6 seconds for a 60-frame volume. The excitation power measured before the entrance pupil of O1 was 1 mW, giving an irradiance at the focal plane of 30 $\mu W \mu m^{-2}$. Sequential acquisition of two channels was acquired, and channels were subsequently combined computationally using ImageJ.[68]

Image Deskewing

Acquired images were deskewed to correct for oblique imaging geometry. The deskewing process was implemented based on the code provided by the QI2lab on GitHub (https://github.com/QI2lab/OPM/tree/master).[45] This approach corrected the image stacks by realigning the oblique planes, resulting in a corrected 3D volume. Using this code, the angle and step size of the light sheet were accounted for, enabling accurate reconstruction of the imaged neurons. The deskewed images were processed and combined for downstream analysis in ImageJ.

Beads samples and PSF measurements:

Beads samples were made on commercial glass slides. The glass first underwent a cleaning process: it was rinsed with acetone and abundant distilled water, sonicated in a 0.2% Hellmanex solution for ten minutes, and dried at 100°C. Then, the glass was positively charged using poly-

(diallyl-dimethylammonium chloride) (PDDA, Sigma-Aldrich, MW ≈ 400–500 kg mol^{-1}). They were immersed in a solution of 1 mg/ml PDDA in 0.5 M NaCl. Finally, a drop containing the beads was deposited on the glass for a few minutes and rinsed with water afterwards. The beads solution was 40 nm, 505/515, Invitrogen for the 488 nm laser characterization, and 100 nm, 580/605, Invitrogen for the 561 nm laser characterization.

The fabricated sample was used to characterize the PSF. Although the SOLS microscope acquires volumes, the beads sample has emitters on a single plane. Therefore, by acquiring a volume, only information from the PSF at the sample position is obtained. Figure S1a shows an example of one of the acquired images.

After acquisition and deskewing, only the frame corresponding to the axial position of the sample was analysed, using the software Picasso.[69] This software localizes the emitters and fits a 2d Gaussian function for each emitter. Figure S1b shows a histogram of the measured values. The PSF in the z-axis was calculated using the PSFj software with the same set of data.[70]

Decorrelation analysis : To estimate the achieved resolution, a parameter-free estimation based on the decorrelation analysis presented by Descloux was employed.[71] The analysis was performed over the z-stack presented in Figure 3b. Figure S1 shows the lateral resolution as a function of the depth within the sample. Within the range of 4 µm, the resolution remains approximately constant at 544 nm with a standard deviation of 32 nm.

References

1. Schlegel, P. *et al.* Whole-brain annotation and multi- connectome cell typing of Drosophila. *Nature* **634**, (2024).

2. Wilson, R. I., Turner, G. C. & Laurent, G. Transformation of Olfactory Representations in the Drosophila Antennal Lobe. *Science (80-.).* **303**, 366–370 (2004).

3. Huang, C. *et al.* Long-term optical brain imaging in live adult fruit flies. *Nat. Commun.* **9**, 1–10 (2018).

4. Sinha, S. *et al.* High-speed laser microsurgery of alert fruit flies for fluorescence imaging of neural activity. *Proc. Natl. Acad. Sci.* **110**, 18374–18379 (2013).

5. Hsu, K.-J., Lin, Y.-Y., Chiang, A.-S. & Chu, S.-W. Optical properties of adult Drosophila brains in one-, two-, and three-photon microscopy. *Biomed. Opt. Express* **10**, 1627 (2019).

6. Chen, Z., Truong, T. M. & Ai, H. W. Illuminating brain activities with fluorescent protein-based biosensors. *Chemosensors* **5**, 1–28 (2017).

7. Lin, A. *et al.* Imaging whole-brain activity to understand behaviour. *Nat. Rev. Phys.* **4**, 292–305 (2022).

8. Lemon, W. C. *et al.* Whole-central nervous system functional imaging in larval Drosophila. *Nat. Commun.* **6**, (2015).

9. Mann, K., Gallen, C. L. & Clandinin, T. R. Whole-Brain Calcium Imaging Reveals an Intrinsic Functional Network in Drosophila. *Curr. Biol.* **27**, 2389-2396.e4 (2017).

10. Górska-Andrzejak, J. *et al.* Circadian expression of the presynaptic active zone protein bruchpilot in the lamina of Drosophila melanogaster. *Dev. Neurobiol.* **73**, 14–26 (2013).

11. Fernández, M. P., Berni, J. & Ceriani, M. F. Circadian Remodeling of Neuronal Circuits Involved in Rhythmic Behavior. *PLOS Biol.* **6**, e69 (2008).

12. Gorostiza, E. A., Depetris-Chauvin, A., Frenkel, L., Pírez, N. & Ceriani, M. F. Circadian pacemaker neurons change synaptic contacts across the day. *Curr. Biol.* **24**, 2161–2167 (2014).

13. Duhart, J. M. *et al.* Modulation and neural correlates of postmating sleep plasticity in Drosophila females. *Curr. Biol.* **33**, 2702-2716.e3 (2023).

14. Wang, Q. *et al.* Optical control of ERK and AKT signaling promotes axon regeneration and functional recovery of PNS and CNS in Drosophila. *Elife* **9**, e57395 (2020).

15. Sivachenko, A., Li, Y., Abruzzi, K. C. & Rosbash, M. The transcription factor Mef2 links the Drosophila core clock to Fas2, neuronal morphology, and circadian behavior. *Neuron* **79**, 281–292 (2013).

16. Herrero, A. *et al.* Coupling Neuropeptide Levels to Structural Plasticity in Drosophila Clock Neurons. *Curr. Biol.* **30**, 3154-3166.e4 (2020).

17. Grienberger, C., Giovannucci, A., Zeiger, W. & Portera-Cailliau, C. Two-photon calcium imaging of neuronal activity. *Nat. Rev. Methods Prim.* **2**, (2022).

18. Sinha, S. *et al.* Principles of Two-Photon Excitation Microscopy and Its Applications to Neuroscience. **110**, 823–839 (2013).

19. Isaacman-Beck, J. *et al.* SPARC enables genetic manipulation of precise proportions of cells. *Nat. Neurosci.* **23**, 1168–1175 (2020).

20. Wang, J. W., Wong, A. M., Flores, J., Vosshall, L. B. & Axel, R. Two-photon calcium

imaging reveals an odor-evoked map of activity in the fly brain. *Cell* **112**, 271–282 (2003).

21. Pacheco, D. A., Thiberge, S. Y., Pnevmatikakis, E. & Murthy, M. Auditory activity is diverse and widespread throughout the central brain of Drosophila. *Nat. Neurosci.* **24**, 93–104 (2021).
22. Lu, R. *et al.* Video-rate volumetric functional imaging of the brain at synaptic resolution. *Nat. Neurosci.* **20**, 620–628 (2017).
23. Leong, J. C. S., Esch, J. J., Poole, B., Ganguli, S. & Clandinin, T. R. Direction selectivity in drosophila emerges from preferred-direction enhancement and null-direction suppression. *J. Neurosci.* **36**, 8078–8092 (2016).
24. Seelig, J. D. *et al.* Two-photon calcium imaging from head-fixed Drosophila during optomotor walking behavior. *Nat. Methods* **7**, 535–540 (2010).
25. Brezovec, B. E. *et al.* Mapping the neural dynamics of locomotion across the Drosophila brain. *Curr. Biol.* **34**, 710-726.e4 (2024).
26. Tainton-Heap, L. A. L. *et al.* A Paradoxical Kind of Sleep in Drosophila melanogaster. *Curr. Biol.* **31**, 578-590.e6 (2021).
27. Münch, D., Goldschmidt, D. & Ribeiro, C. *The neuronal logic of how internal states control food choice*. *Nature* vol. 607 (Springer US, 2022).
28. Mann, K., Deny, S., Ganguli, S. & Clandinin, T. R. Coupling of activity, metabolism and behaviour across the Drosophila brain. *Nature* **593**, 244–248 (2021).
29. Picot, A. *et al.* Temperature Rise under Two-Photon Optogenetic Brain Stimulation. *Cell Rep.* **24**, 1243-1253.e5 (2018).
30. Donovan, E. J. *et al.* Dendrite architecture determines mitochondrial distribution patterns in vivo. *Cell Rep.* **43**, 114190 (2024).
31. Delestro, F. *et al.* In vivo large-scale analysis of Drosophila neuronal calcium traces by automated tracking of single somata. *Sci. Rep.* **10**, 1–14 (2020).
32. Harris, D. T., Kallman, B. R., Mullaney, B. C. & Scott, K. Representations of Taste Modality in the Drosophila Brain. *Neuron* **86**, 1449–1460 (2015).
33. Aimon, S., Cheng, K. Y., Gjorgjieva, J. & Kadow, I. C. G. *Global change in brain state during spontaneous and forced walk in drosophila is composed of combined activity patterns of different neuron classes*. *eLife* vol. 12 (2023).
34. Aimon, S. *et al. Fast near-whole-brain imaging in adult drosophila during responses to stimuli and behavior*. *PLoS Biology* vol. 17 (2019).
35. Lu, Z. *et al.* Long-term intravital subcellular imaging with confocal scanning light-field microscopy. *Nat. Biotechnol.* (2024).
36. Hillman, E. M. C., Voleti, V., Li, W. & Yu, H. Light-Sheet Microscopy in Neuroscience. *Annu. Rev. Neurosci.* **42**, 295–313 (2019).
37. Stelzer, E. H. K. *et al.* Light sheet fluorescence microscopy. *Nat. Rev. Methods Prim.* **1**, (2021).
38. Ahrens, M. B., Orger, M. B., Robson, D. N., Li, J. M. & Keller, P. J. Whole-brain

functional imaging at cellular resolution using light-sheet microscopy. *Nat. Methods* **10**, 413–420 (2013).

39. Liang, X., Holy, T. E. & Taghert, P. H. Synchronous Drosophila circadian pacemakers display nonsynchronous Ca2+ rhythms in vivo. *Science (80-.).* **351**, 976–981 (2016).

40. Hubert, A. *et al.* Enhanced neuroimaging with a calcium sensor in ex-vivo Drosophila melanogaster brains using closed-loop adaptive optics light-sheet fluorescence microscopy. *J. Biomed. Opt.* **28**, (2023).

41. Bouchard, M. B. *et al.* Swept confocally-aligned planar excitation (SCAPE) microscopy for high-speed volumetric imaging of behaving organisms. *Nat. Photonics* **9**, 113–119 (2015).

42. Voleti, V. *et al.* Real-time volumetric microscopy of in vivo dynamics and large-scale samples with SCAPE 2.0. *Nat. Methods* **16**, 1054–1062 (2019).

43. Dunsby, C. Optically sectioned imaging by oblique plane microscopy. *Opt. InfoBase Conf. Pap.* **16**, 186–196 (2009).

44. Kumar, M., Kishore, S., Nasenbeny, J., McLean, D. L. & Kozorovitskiy, Y. Integrated one- and two-photon scanned oblique plane illumination (SOPi) microscopy for rapid volumetric imaging. *Opt. Express* **26**, 13027 (2018).

45. Sapoznik, E. *et al.* A versatile oblique plane microscope for large-scale and high-resolution imaging of subcellular dynamics. *Elife* **9**, 1–39 (2020).

46. Yang, B. *et al.* DaXi—high-resolution, large imaging volume and multi-view single-objective light-sheet microscopy. *Nat. Methods* **19**, 461–469 (2022).

47. Schaffer, E. S. *et al.* The spatial and temporal structure of neural activity across the fly brain. *Nat. Commun.* **14**, (2023).

48. Yang, B. *et al.* Epi-illumination SPIM for volumetric imaging with high spatial-temporal resolution. *Nat. Methods* **16**, 501–504 (2019).

49. Botcherby, E. J., Juškaitis, R., Booth, M. J. & Wilson, T. An optical technique for remote focusing in microscopy. *Opt. Commun.* **281**, 880–887 (2008).

50. Millett-Sikking, A., Thayer, N. H., Bohnert, A. & York, A. G. calico/remote_refocus: Pre-print. (2018) doi:10.5281/zenodo.1146084.

51. Millett-Sikking, A. & York, A. AndrewGYork/high_na_single_objective_lightsheet: Work-in-progress. (2019) doi:10.5281/ZENODO.3376243.

52. Kumar, M. & Kozorovitskiy, Y. Tilt (in)variant lateral scan in oblique plane microscopy: a geometrical optics approach. *Biomed. Opt. Express* **11**, 3346 (2020).

53. Lvarez, P. A. L. O. Z. A. Light-sheet microscopy : a tutorial. **10**, 111–179 (2018).

54. Stoleru, D., Peng, Y., Nawathean, P. & Rosbash, M. A resetting signal between Drosophila pacemakers synchronizes morning and evening activity. *Nature* **438**, 238–242 (2005).

55. Renn, S. C. P., Park, J. H., Rosbash, M., Hall, J. C. & Taghert, P. H. A pdf neuropeptide gene mutation and ablation of PDF neurons each cause severe abnormalities of behavioral circadian rhythms in Drosophila. *Cell* **101**, 791–802 (2000).

56. Helfrich-Förster, C. & Homberg, U. Pigment-dispersing hormone-immunoreactive neurons in the nervous system of wild-type Drosophila melanogaster and of several mutants with altered circadian rhythmicity. *J. Comp. Neurol.* **337**, 177–190 (1993).

57. Jayaraman, V. & Laurent, G. Evaluating a genetically encoded optical sensor of neural activity using electrophysiology in intact adult fruit flies. *Front. Neural Circuits* **1**, 1–9 (2007).

58. Richardson, W. H. Bayesian-Based Iterative Method of Image Restoration*. *J. Opt. Soc. Am.* **62**, 55–59 (1972).

59. Benninger, R. K. P. & Piston, D. W. *Two-photon excitation microscopy for the study of living cells and tissues*. *Current Protocols in Cell Biology* (2013).

60. Peres, C., Nardin, C., Yang, G. & Mammano, F. Commercially derived versatile optical architecture for two-photon STED, wavelength mixing and label-free microscopy. *Biomed. Opt. Express* **13**, 1410–1429 (2022).

61. Sparks, H., Almagro, J., Behrens, A., Salbreux, G. & Dunsby, C. Dual-view oblique plane microscopy. *Opt. InfoBase Conf. Pap.* **11**, 7204–7220 (2021).

62. Chen, B. *et al.* Projective light-sheet microscopy with flexible parameter selection. *Nat. Commun.* **15**, 1–8 (2024).

63. Guo, K., Kalyviotis, K., Pantazis, P. & Rowlands, C. J. Hyperspectral oblique plane microscopy enables spontaneous, label-free imaging of biological dynamic processes in live animals. *Proc. Natl. Acad. Sci. U. S. A.* **121**, 1–9 (2024).

64. Chen, B. *et al.* Resolution doubling in light-sheet microscopy via oblique plane structured illumination. *Nat. Methods* **19**, 1419–1426 (2022).

65. Mcfadden, C. *et al.* Adaptive optics in an oblique plane microscope. *Biomed. Opt. Express* **15**, 4498 (2024).

66. Park, D., Li, P., Dani, A. & Taghert, P. H. Peptidergic Cell-Specific Synaptotagmins in Drosophila: Localization to Dense-Core Granules and Regulation by the bHLH Protein DIMMED. *J. Neurosci.* **34**, 13195 LP – 13207 (2014).

67. Fujiwara, T., Brotas, M. & Chiappe, M. E. Walking strides direct rapid and flexible recruitment of visual circuits for course control in Drosophila. *Neuron* **110**, 2124-2138.e8 (2022).

68. Rueden, C. T. *et al.* ImageJ2: ImageJ for the next generation of scientific image data. *BMC Bioinformatics* **18**, 1–26 (2017).

69. Schnitzbauer, J., Strauss, M. T., Schlichthaerle, T., Schueder, F. & Jungmann, R. Super-resolution microscopy with DNA-PAINT. *Nat. Protoc.* **12**, 1198–1228 (2017).

70. Theer, P., Mongis, C. & Knop, M. PSFj: know your fluorescence microscope. *Nat. Methods* **11**, 981–982 (2014).

71. Descloux, A., Grußmayer, K. S. & Radenovic, A. Parameter-free image resolution estimation based on decorrelation analysis. *Nat. Methods* **16**, 918–924 (2019).

Acknowledgments

We thank Lucía Lopez, Gonzalo Escalante, Alan Szalai, and Fernando Stefani for support and materials.

We thank Alfred Millett-Sikking, Kayley Hake, Juan Carlos Boffi, Luciano Masullo and Andrew York for insightful advice and discussions.

We thank Eugenia Chiappe for tips and training on sample preparation.

F.J.T. holds a fellowship from the National Agency for the Promotion of Science, Technology and Innovation (Agencia I+D+i). J.I.I., M.RC are supported by graduate fellowships from the Argentine Research Council for Science and Technology (CONICET); J.G. and M.F.C. are members of CONICET; This work was supported by the PICT2018-0995 (to M.F.C.) from Agencia I+D+i, Argentina and by R01NS108934 (to H. delaI., M.E. and M.F.C.). The funders had no role in study design, data collection and analysis, decision to publish, or preparation of the manuscript.

Author contributions:

Research conception: M.F.C.

Microscope design: M.B. and J.G

Microscope building and alignment: F.J.T. and J.G.

Software development for microscope control: F.J.T.

Data acquisition: F.J.T., L.S, M.F, M.RC, J.I.I. and J.G.

Data analysis: F.J.T., M.B. L.S, M.F, and J.G.

Supervision and Funding: M.E., H.O.I, and M.F.C.

Fly Pushing and dissection: F.J.T., M.RC, and J.I.I.

Writing—original draft: M.B., and J.G.

Figures: F.J.T., M.B, L.S, M.F, and J.G.

Writing—review & editing: All authors.

Competing interests:

The authors declare that they have no competing interests.

Data and materials availability:

All data generated or analyzed during this study are included in this published article (and its supplementary information files).